remote sensing

MDPI

Article

Millimeter-Wave Radar Detection and Localization of a Human in Indoor Complex Environments

Zhixuan Xing [1], Penghui Chen [1,*], Jun Wang [1,2], Yujing Bai [1], Jinhao Song [1] and Liuyang Tian [1]

[1] School of Electronic and Information Engineering, Beihang University, Beijing 100191, China; zhixuanxing@buaa.edu.cn (Z.X.); wangj203@buaa.edu.cn (J.W.); baiyvjing@buaa.edu.cn (Y.B.); jh_song@buaa.edu.cn (J.S.); liuyangtian@buaa.edu.cn (L.T.)
[2] Hangzhou Innovation Institute, Beihang University, Hangzhou 310056, China
* Correspondence: chenpenghui@buaa.edu.cn

Abstract: Nowadays, it is still a great challenge to detect and locate indoor humans using a frequency-modulated continuous-wave radar accurately. Due to the interference of the indoor environment and complex objects such as green plants, the radar signal may penetrate, reflect, refract, and scatter, and the echo signals will contain noise, clutter, and multipath of different characteristics. Therefore, a method combined with comprehensive non-target signal removal and human localization is proposed to achieve position estimation of a human target. Time-variant clutter is innovatively mitigated through time accumulation using point clustering. Ghost targets are reduced according to propagation path matching. The experimental results show that the method can locate the real target human within an average error of 0.195 m in multiple complex environments with green plants, curtains, or furniture using a 77 GHz millimeter-wave radar. Meanwhile, the proposed method performs better than conventional methods. The detection probability is 81.250% when the human is behind a potted plant and is 90.286% when beside it.

Keywords: clutter removal; human detection; indoor localization; multipath suppression

Citation: Xing, Z.; Chen, P.; Wang, J.; Bai, Y.; Song, J.; Tian, L. Millimeter-Wave Radar Detection and Localization of a Human in Indoor Complex Environments. *Remote Sens.* **2024**, *16*, 2572. https://doi.org/10.3390/rs16142572

Academic Editor: Piotr Samczynski

Received: 27 May 2024
Revised: 5 July 2024
Accepted: 12 July 2024
Published: 13 July 2024

1. Introduction

With the rapid development of smart homes, smart communities, and so on, human target recognition using radars has been widely discussed recently. Compared to cameras [1–3] and wearable devices [4–6] the use of radar is more convenient and can protect personal privacy. What is more, effective information can be gained even at night using a radar. Therefore, the use of radars for indoor human sensing in the field of smart+ has become a research hotspot [7–12].

Compared with an outdoor environment, an indoor environment is more complex. Electromagnetic waves are reflected from the ceiling, walls, floors, and other indoor objects. This will generate ghost targets that have similar characteristics to a real target and generate false alarms in target detection. As for multipath removal, common methods can be divided into two types including methods based on data and methods based on models [13]. Methods based on data use a machine learning or deep neural network to classify real and ghost targets. A classifier based on a deep neural network was proposed in [14] and gained an accuracy of 87.36% on average. However, this kind of method has insufficient ghost target datasets and higher computation complexity. As for methods based on models, the weighted entropy [15] was used to improve detection accuracy. After that, a time-differential channel was used to calculate the element difference [16] and then mitigate non-target signals. The methods of least squares and the non-line of sight (NLOS) [17] were applied under static and mobile modules. Then, a multiple-input and multiple-output (MIMO) radar and the Hough transform were used to detect range-Doppler (RD) maps [18]. The experimental results showed that the method was effective in suppressing multipath false targets and detecting a walking human. A hybrid clutter model-based

LMB (HCM-LMB) filter [19] which incorporates the spatial and temporal properties of clutter was designed to filter the multipath signal in pedestrian number identification. Echo signal propagation was used in [20], and the multipath-assisted localization (MAL) model determines the radar sensing area by analyzing the signal interaction influenced by ghost signals. To develop it further, a false target-matching elimination method for multipath suppression was proposed [21], and the experimental results showed that the method was effective in urban road environments. The echo signal multipath model has great robustness and low computation complexity, and it is popular in multipath mitigation.

At the same time, plants are a kind of complex medium for electromagnetic wave propagation. When the radar transmits signals passing through the leaves and branches of plants, part of the signals passes through the gap or penetrates the leaves, and part of the signals will be reflected, refracted, and scattered. Meanwhile, another part of the signals will be absorbed by the plant. These will cause echo signals to be interfered with and attenuate and make the multipath effect more complex. In addition, it is difficult to identify the real target because of the low radar cross-section (RCS) of the human and the similarity between the frequency and characteristics of the human and the plant [22]. So, green plants will be discussed individually among various indoor objects.

There exists research focusing on target detection and wooded environments. A propagation channel model in a foliage environment was characterized for better target detection in [23]. Wind was taken into account, and woods were considered as non-static objects in [24]. Ultra-wideband radars were used to detect the human. A classification algorithm [25] was selected based on high-order cumulant (HOC) to make the characteristics of humans and dogs more distinct. Then, the method could distinguish between humans and dogs through pulsed radio ultra-wideband signals. As for human detection and localization, the low-frequency broadband radars and the entropy-weighted coherent integration (EWCI) algorithm [26] were used to filter multipath generated by reflection on rough trunks with large fluctuations. However, in an indoor environment with a potted plant, multipath signals have fewer fluctuations, and the method in [26] is not suitable. In [27], the exponential average background subtraction (EABS) method was used to filter out the background noise adaptively. A window filter was applied to solve the problem of several range cell distributions of one target. Through ultra-high-frequency (UHF) band radar echoes, moving humans can be detected. In [28], the Doppler-compensated angle was calculated, and an SVM classifier was used to remove ghost targets. However, machine learning has a higher computation complexity. It can be seen that few pieces of research comprehensively focus on noise, clutter, and multipath removal for human detection and localization in a complex environment, especially in a wooded environment. Using a millimeter-wave radar indoors with potted plants, a more accurate detection of static human targets is still a difficult task.

Therefore, range and azimuth angle calculation and filtering methods of noise, clutter, and multipath were exploited. Then, the localization of indoor static human targets was achieved, which is shown in Figure 1. It was tested in multiple environments with green plants, curtains, and furniture and was compared with the conventional methods in [21,27,28].

The main contributions can be summarized as follows.

To detect a static human target indoors in complex environments, especially with green plants, a very comprehensive method was carried out to analyze the removal of static noise, dynamic clutter, and multipath false targets and target localization only based on one single millimeter-wave radar. The proposed method was evaluated in five complex real scenarios with potted plants, curtains, and furniture. Results showed that the average localization error is within 0.195 m and performed better than the two conventional methods.

To mitigate the effect of slight changes in the human body and remove time-varying clutter, a dynamic clutter removal method was innovatively proposed considering the characteristics of static human targets. It combined DBSCAN clustering for a long-time

accumulation and binary integration. The method could classify points with small fluctuations into the same target.

To remove the effect of multipath reflected from indoor objects, a signal propagation model was analyzed, and multipath matching was used. Experiments verified the broad applicability and high detection accuracy of the method with a low computation complexity.

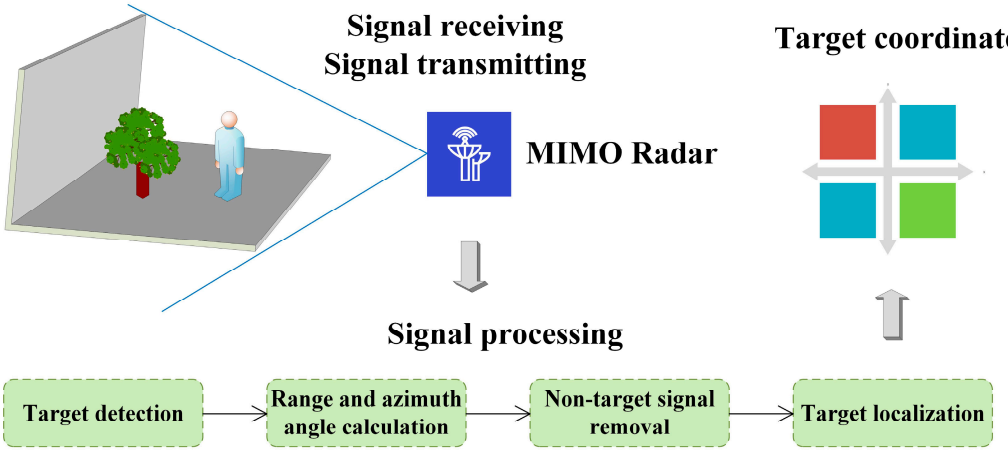

Figure 1. The overall structure design of the human detection and localization system.

2. The Radar Signal Model

The frequency-modulated continuous-wave (FMCW) radar signal is sampled by an analog-to-digital converter (ADC) and can be expressed as $S_b(n, m, l, f)$, where n denotes the index of sampling points in the fast time dimension and there are N sampling points in total. m denotes the index of chirps in the slow time dimension and there are M chirps. l denotes the index of channels, and the number of virtual channels is

$$L = N_{tx} N_{rx} \tag{1}$$

where N_{tx} is the number of transmitting antennas and N_{rx} is the number of receiving antennas. f denotes the number of frames, and there are totally F frames.

During one frequency-modulation cycle T_c of a radar, the transmitted signal at Tx is

$$S_t(t) = A\cos[j(2\pi f_c t + \pi S t^2)], 0 \le t \le T_c \tag{2}$$

where t represents the time, A represents the amplitude of the transmitted signal, f_c represents the signal carrier frequency, S represents the frequency-modulated slope of a chirp, and T_c represents the frequency-modulated period of a chirp. For a target at a distance R from the radar, it takes time τ for the signal propagation from transmission to receiving. Ignoring the amplitude change of the signal, the radar echo signal at Rx can be expressed as

$$\begin{aligned} S_r(t) &= S_t(t-\tau) \\ &= A\cos\left\{j[2\pi f_c(t-\tau) + \pi S(t-\tau)^2]\right\} \end{aligned} \tag{3}$$

As for a static target, the signal round-trip delay is

$$\tau = \frac{2R}{c} \tag{4}$$

where c represents the speed of light.

When the target stays still, mix the transmitted signal and the received signal of the radar, and the beat signal is

$$S_b(t) = A^2\cos\left\{j2\pi[\frac{2SR}{c}t + \frac{2f_cR}{c} - \frac{2SR^2}{c^2}]\right\} \tag{5}$$

For the target, the frequency difference is

$$f_{\mathrm{b}} = \frac{2SR}{c} \tag{6}$$

By performing 1D FFT on the radar signal, the frequency difference f_{b} can be obtained and then the distance of the target can be calculated as

$$R = \frac{f_{\mathrm{b}} c}{2S} \tag{7}$$

If the target moves at a speed v, mix the transmitted signal and the received signal, and higher-order terms are removed after low-pass filtering. The beat signal is

$$S_{\mathrm{b}}(t) = A^2 \cos\left\{ j2\pi[(\frac{2SR}{c} + \frac{2f_c v}{c})t + \frac{2f_c R}{c} - \frac{2SR^2}{c^2}] \right\} \tag{8}$$

The phase difference of the signal between each chirp can be expressed as

$$\Delta\varphi = \frac{4\pi v \Delta t}{\lambda} \tag{9}$$

where λ denotes the wavelength of the radar signal and Δt denotes the time interval between the transmitted chirps.

So, the speed can be expressed as

$$v = \frac{\lambda \Delta\varphi}{4\pi M T_{\mathrm{c}} N_{\mathrm{tx}}} \tag{10}$$

For the uniform antenna array of an FMCW radar, the spacing of adjacent channels is d, the signal arrives at an angle θ, and the propagation distance difference between adjacent antennas can be expressed as $d \sin\theta$, thus the angle of the target is obtained

$$\theta = \sin^{-1}(\frac{\lambda\omega}{2\pi d}) \tag{11}$$

where ω denotes the phase difference of the signal between each channel.

3. The Signal Processing Overall Design

In a real indoor experiment with a potted plant, the beat signal contains noise, time-variant signals, and false targets generated by multipath in addition to the target S_{b}

$$S'_{\mathrm{b}}(t) = S_{\mathrm{b}}(t) + \sum_{i=1}^{N_{\mathrm{m}}} \alpha_i S_{\mathrm{b}}(t - \tau_i) + \mu(t) + \delta \tag{12}$$

where $\sum_{i=1}^{N_{\mathrm{m}}} \alpha_i S_{\mathrm{b}}(t - \tau_i)$ denotes multipath, N_{m} denotes the number of multipath ghost targets, α_i denotes the amplitude gain of the ith multipath, τ_i denotes the round-trip delay time of the ith multipath, $\mu(t)$ denotes time-variant clutter, and δ denotes static noise. Thus, these need to be filtered.

Therefore, the flow chart of the signal processing overall design is shown in Figure 2. Firstly, averaging filtering [29] is performed on the echo signals collected by the radar to remove static noise, and then the fast Fourier transform [30] is performed in both the distance and velocity dimensions to obtain high-resolution range profiles (HRRPs) and RD maps. The constant false alarm rate (CFAR) algorithm [31] is applied to the RD maps to detect the presence of a target. The peaks in the data are searched [32,33], and then the Capon algorithm [34] is applied to estimate angles to calculate the coordinate information. The density-based spatial clustering of applications with noise (DBSCAN) algorithm [35]

and binary integration [36] are applied to further remove time-variant clutter and to obtain all possible target points. The multipath locations are analyzed [21] to eliminate false targets, to identify the presence of the human, and to obtain location by FMCW radar.

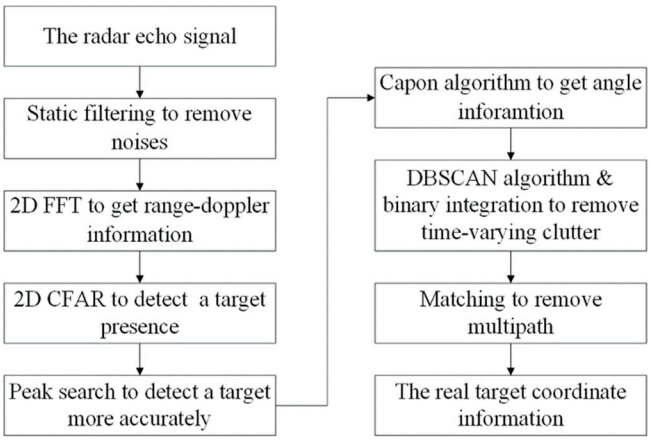

Figure 2. The signal processing overall system.

The complete process of noise, clutter, and multipath filtering is shown in Figure 3. The radar echo signal is time-variant and non-smooth, and the position of the non-target signal is random with mutations. Meanwhile, the frequency components are not single, and the multipath effect results in similar characteristics between the ghost targets and the real targets. Static filtering can initially filter out static noise. The DBSCAN algorithm can filter out clutter with fluctuations or random appearances in the position. The binary integration parameters are determined by the existence times of a target. A target exists when the value of times the target appears in the same position is greater than or equal to the set threshold. Therefore, time-variant clutter can be filtered out based on these characteristics. At the same time, according to the principle of specular reflection, the multipath effect can be removed by matching theoretical positions with the suspected targets.

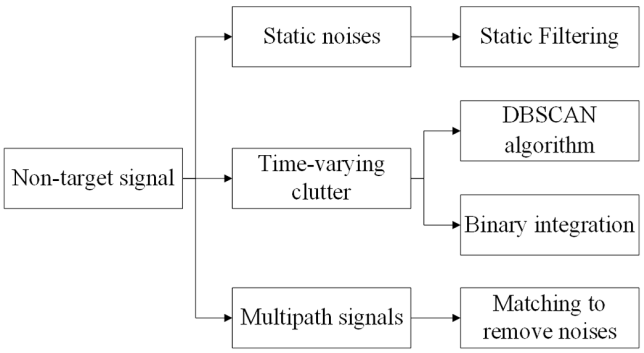

Figure 3. The overall design for noises, clutter, and multipath false target filtering.

After removing noise, time-variant clutter, and multipath signals according to Figure 3, the estimated signal containing a static target is

$$\hat{S}_{\mathrm{b}}(t) \approx S_{\mathrm{b}}(t) = A^2 \cos\left\{ j2\pi\left[\frac{2SR}{c}t + \frac{2f_{\mathrm{c}}R}{c} - \frac{2SR^2}{c^2}\right]\right\} \tag{13}$$

where A denotes the amplitude of the signal, S denotes the slope of the chirp signal, R denotes the distance between the target and the radar, c denotes the speed of light, t denotes the time, and f_c denotes the signal carrier frequency.

4. Potential Challenges and Solutions

4.1. Low Signal-to-Noise Ratio (SNR) for Static Human Targets

Static human detection presents a significant challenge due to inherently weak radar signal reflections and a low SNR of the received signals. Unlike walking humans, static human targets do not generate strong Doppler shifts, which are typically used to distinguish targets from background noise and clutter. As a result, the amplitudes of reflected radar signals are sometimes weak and can be easily overwhelmed by noise and time-varying clutter.

Therefore, long-term signal integration is used in the process. After continuously collecting radar data, averaging filtering was applied instead of other noise removal methods, such as moving target indication (MTI). In this way, a static human with breath and heartbeat can also be recognized. After that, clutter was found in signal data. It appeared randomly and was difficult to remove in a single frame due to weak amplitude. Then, a clustering method using time accumulation is proposed, and the real target can be classified as a target, and false alarms can be classified as clutter.

4.2. Target Parameter Estimation

To obtain accurate detection results, accurate distance and azimuth angle information are needed. As for distance estimation, excessive sampling points can lead to substantial computational complexity, while insufficient sampling points can degrade the accuracy of distance estimation. Through iterative adjustments, a sample size of 256 points was selected, ensuring both manageable computational demands and sufficient accuracy for distance estimation. As for azimuth angle estimation, initially, it was performed using the FFT algorithm. However, this approach exhibited obvious discrepancies between the estimated angles and the actual target angles. To address this, the super-resolution algorithm Capon is implemented. These both significantly improve the accuracy of target parameter estimation.

5. Data Preprocessing and Detection of Possible Targets

5.1. Preprocessing

The averaging filtering is used to filter out static noise, removing the direct current components with zero-distance variation from the reflection of static objects. The signal is averaged, and the average is subtracted from the original signal. The realization process is

$$E(n,m,l) = \frac{1}{F}\sum_{f=1}^{F} \hat{S}_{\mathrm{b}}(n,m,l,f) \tag{14}$$

$$S_1(n,m,l,f) = \hat{S}_{\mathrm{b}}(n,m,l,f) - E(n,m,l) \tag{15}$$

5.2. Target Parameter Estimation

To obtain the distance and azimuth angle information of the target, 2D-FFT, CFAR detection, peak search, and azimuth angle calculation are used.

Two-dimensional (2D)-FFT in the range and Doppler dimension is applied first. Peak search enhances the difference between a target and other signals. The Capon algorithm is applied in the azimuth dimension to obtain more accurate angle information.

5.2.1. 2D-FFT

Carry out two-dimensional fast Fourier transform (2D-FFT) on windowed data $S_{\mathrm{w}}(n,m,l,f)$

$$S_{\mathrm{fft,r}}(k_{\mathrm{s}},m,l,f) = DFT(S_{\mathrm{w}}(n_{\mathrm{fft,r}},m,l,f)) \tag{16}$$

$$S_{\mathrm{fft,d}}(k_{\mathrm{s}},k_{\mathrm{c}},l,f) = DFT(S_{\mathrm{fft,r}}(k_{\mathrm{s}},n_{\mathrm{fft,d}},l,f)) \tag{17}$$

where $n_{\text{fft.r}}$ is the Fourier transform sampling index in the distance dimension and $n_{\text{fft.r}} \in [1, N_{\text{fft,r}}]$. $N_{\text{fft,r}}$ is the sampling total number. $n_{\text{fft,d}}$ is the Fourier transform sampling index in the Doppler dimension and $n_{\text{fft,d}} \in [1, N_{\text{fft,d}}]$. $N_{\text{fft,d}}$ is the total sampling number of that.

5.2.2. CFAR Detection

To determine whether a target exists or not, CFAR detection is used. When there is only clutter in the signal, it makes an assumption H_0. When the signal contains both the target and clutter, it makes an assumption H_1.

As for the assumption H_0, the background is uniform and is composed of clutter only. The signal amplitude follows the exponential distribution, so the power of the signal $P = \xi_0$

$$\xi_0 = \frac{1}{N_{\text{tr}}} \sum_{i=I_1}^{N_{\text{tr}}+I_1-1} P_i \tag{18}$$

where N_{tr} is the number of training cells, and P_i is the interfering signal power of each cell. When the constant false alarm rate is P_{F}, the threshold

$$V_{\text{T}} = -\xi_0 \ln(P_{\text{F}}) \tag{19}$$

As for the assumption H_1, the power of the signal $P = S_0 + \xi_0$. The received signal $S_{\text{fft,d}}$ is compared with the threshold. If it is higher than the threshold, then the target exists, and the original signal remains unchanged. If it is lower, then there is no target and the signal is set to zero. After that, the CFAR processed signal S_{cfar} and the unit location of the target V_{cfar} are combined.

Common averaging and ordered statistics CFAR detection methods include smallest of (SO)-CFAR detection, cell averaging (CA)-CFAR detection, greatest of (GO)-CFAR detection, and ordered statistics (OS)-CFAR detection. The GO-CFAR detection performs well in the edge of clutter, which is suitable for target detection in the Doppler dimension. The OS-CFAR detection method has great performance in an adjacent multi-target environment. Therefore, OSGO-CFAR is chosen.

5.2.3. Peak Search

Peak search is implemented as shown in Figure 4. By searching, if the amplitude of a point is greater than that of the previous sampling point, the next sampling point, the previous chirp, and the next chirp, then the signal, the corresponding sampling point, and the chirp indexes are recorded. Meanwhile, target signals S_{tar} and positions V_{tar} are obtained.

Peak Searching

Data: Signals S_{cfar}, CFAR positions V_{cfar}
Result: Target signals S_{tar}, Target positions V_{tar}
while *there is a possible target in* S_{cfar} **do**
  According to the signal S_{cfar} and CFAR position V_{cfar};
  The possible target is set as S_{middle};
  The previous one in the range dimension is set as S_{up};
  The next one in the range dimension is set as S_{down};
  The previous one in the doppler dimension is set as S_{left};
  The next one in the doppler dimension is set as S_{right};
  if *the amplitude of the middle signal is maximum* **then**
    Let S_{tar} be the signal S_{middle};
    Let V_{tar} be the position of the middle signal;
  else
    Nothing;
  end
end

Figure 4. Implementation Process of Peak Search.

5.2.4. Azimuth Angle Calculation

The Capon algorithm is applied to estimate the azimuth angle. The radar has a uniform array of L_{azi} virtual antennas for horizontal angle estimation, and the number of azimuth searching points is N_{azi}. The steering vector can be expressed as

$$\omega(\theta_i) = \chi_i C^{-\mathbf{1}} a(\theta_i) \tag{20}$$

where $i \in [1, N_{\text{azi}}]$, χ_i denotes constant energy at a certain search angle θ_i, the covariance of the signal constitutes the matrix C, and $a(\theta_i)$ denotes the direction vector.

Calculate the covariance matrix for each frame

$$C(l_1, l_2) = \frac{S_{\text{tar}}^{\text{H}}(k_{c_1}, l_1) S_{\text{tar}}(k_{c_2}, l_2)}{N_{\text{fft,d}}} \tag{21}$$

where $k_{c_1}, k_{c_2} = 1, 2, \ldots, N_{\text{fft,d}}$ are the chirp indexes and $l_1, l_2 = 1, 2, \ldots, L_{\text{azi}}$ are the azimuth channel indexes.

Thus, the energy at each angle is

$$\chi_i = \frac{1}{a^{\mathbf{H}}(\theta_{\mathbf{i}}) C^{-\mathbf{1}} a(\theta_{\mathbf{i}})} \tag{22}$$

Searching for the maximum energy, the corresponding angle is the estimated value.

5.3. Clutter Suppression

In real life, people are not absolutely static and result in time-variant signals. First, breathing, heartbeat, and other physiological activities make the human body have a gentle rise and fall beyond a range cell. Second, although people stand still, they have a slight sway. Meanwhile, the complex structure of a potted plant and the occasional instability of a radar make the time variability of the passing signal more obvious. Therefore, the echo signal contains time-variant clutter, which needs to be suppressed. Signals with small position fluctuations need to be categorized as the same target.

When clutter suppression is performed on the static target human signal, the signal strength is relatively low, and there is no Doppler shift, so it is more difficult to distinguish the human target from the non-target signal. Therefore, a method combining the DBSCAN algorithm with binary accumulation is proposed. According to the characteristics of small changes in target position, time accumulation is innovatively used to enhance the static target signal and suppress time-varying clutter.

5.3.1. Calculation of Coordinates

Establish a rectangular coordinate system, and set the coordinate of the radar as the origin O (0, 0). According to the distance R_{tar} between the target and the radar, and the azimuth angle θ_{tar} of the target, a coordinate $(x_{\text{tar}}(i), y_{\text{tar}}(i))$ can be obtained under each frame.

$$x_{\text{tar}}(i) = R_{\text{tar}}(i) \sin \theta_{\text{tar}}(i) \tag{23}$$

$$y_{\text{tar}}(i) = R_{\text{tar}}(i) \cos \theta_{\text{tar}}(i) \tag{24}$$

where $i \in [1, F]$.

5.3.2. The DBSCAN Algorithm

Long-time accumulation is needed to improve the detection accuracy and suppress the time-varying clutter effect. Clustering can accumulate radar echo signals for a long time, and time consistency can be used to weaken the influence of clutter signals. After CFAR detection and peak search, the number of false targets generated by multipath is unknown. Density clustering algorithms do not need to pre-set the number of clusters; thus, the DBSCAN algorithm is selected.

The DBSCAN algorithm has two parameters that can describe the degree of clustering: the domain radius threshold ε of Equation (1) in [37] and the minimum number (MinPts) of points [35]. Data points can be divided into three types: core points, border points, and noise. If the number of data points within the ε is no less than the MinPts, then these data points are classified as core points. If the number of data points within the ε is less than the MinPts, but they are within the ε distance of core points, then these data points are border points. The remaining points belong to noise. The calculation process is achieved as follows. First, mark "not visited" for every input data point. Choose the radius ε and MinPts. Then, choose a "not visited" data point randomly. If the number of points within its ε distance is larger than the MinPts, then classify the selected point as a core point. Create a cluster for it. If not, classify it as a border point. Mark the selected point as "visited". Third, for all points in the ε-neighborhood of the core point, mark them as "visited". Retrieve the ε-neighborhood of these points until there are no other points that are added to the cluster. Finally, repeat Steps 2 and 3 until all points have "visited" marks. If data points in a cluster are all border points, then the data points are classified as noise.

Considering slight body sway and human body width, if three adjacent distance cells exist targets, then they are considered the same target. The value of 1.5 times of a distance cell is chosen. It is selected as the parameter domain radius threshold ε. The selection of the parameter minimum number (MinPts) of points is based on the theory of binary accumulation. Points with large fluctuations as well as random variations are determined as clutter and all possible targets are categorized into N_{PosTar} clusters.

5.3.3. Binary Integration

To detect targets more correctly, binary integration is applied to eliminate the effect of residual clutter, and it is also called M/N detection.

The process involves two hypotheses: "target present" or "target absent", so the result is binary. When detecting a target for N times, the result may be correct or incorrect every time. The criterion M out of N times detection can improve the detection reliability. Traditional ideas use N times only for detection and decision-making without considering another parameter M, and binary integration effectively eliminates the effects of non-target signals and rare detection errors. The decision criterion results in a more robust detection process and is flexible because it can be adapted to different conditions by adjusting the number of M.

After performing the peak search for N times, N decision results are generated, and the target is considered to be present when the target is at the same location for M times or more than M times. Here, the total decision times $N = F$, F is the number of frames of the acquired signal. For the selection of M, a smaller one increases the false alarm rate, and a larger one affects the detection performance. So, the number $M = N/2$ is selected. The location information is saved when the number of appearance times M is greater than or equal to $N/2$, and it can be concluded that a suspected target exists in the current location. Therefore, the parameter $MinPts = N/2 = F/2$.

6. Multipath Ghost Target Analysis and Removal

Based on the results after clustering, the average of points is calculated to represent the coordinate of each cluster

$$(x_n, y_n) = [mean(x_{\mathrm{tar}}(n)), mean(y_{\mathrm{tar}}(n))] \tag{25}$$

where $n \in [1, N_{\mathrm{PosTar}}]$. Put all cluster coordinates into a vector

$$\boldsymbol{x_{PosTar}} = [x_1, x_2, \ldots x_n, \ldots, x_{N_{\mathrm{PosTar}}}] \tag{26}$$

$$\boldsymbol{y_{PosTar}} = [y_1, y_2, \ldots y_n, \ldots, y_{N_{\mathrm{PosTar}}}] \tag{27}$$

Multipath propagation paths and false ghosts are analyzed and then can be mitigated through it.

6.1. Multipath Propagation Analysis

In indoor environments, ceilings, floors, walls, furniture, terylene curtains, and plants are smooth. According to Equation (28), the signal wavelength is calculated to be 3.896 mm for a radar with the start frequency $f_0 = 77$ GHz. Compared to the signal wavelength, their surfaces have little undulation, so specular reflection occurs and thus produces a multipath effect.

$$\lambda = c/f_0 \tag{28}$$

Due to the complex structure of green plants, and because they are widely arranged indoors, plants are discussed mostly. Other indoor obstacles such as walls and furniture result in similar multipath propagation paths or less.

6.1.1. A Human beside a Potted Plant

Take plants as an example to analyze the case of a single reflector, and take plants and walls as an example to analyze the case of two reflectors. Draw multipath propagation schematics. Figure 5a is the case of a single reflector, and Figure 5b is the case of two reflectors. As for three or more reflectors, the attenuation of radar signal propagation is large, and the multipath effect is not considered.

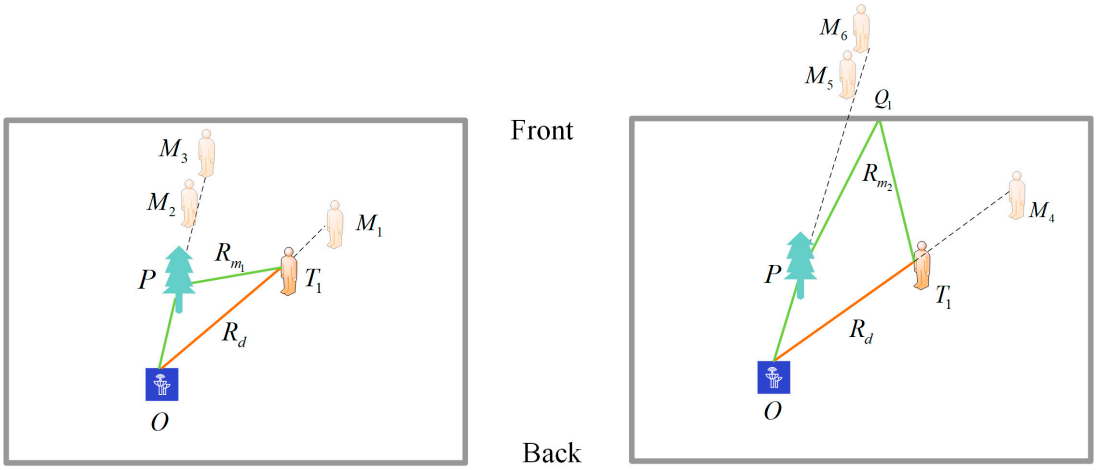

(**a**) (**b**)

Figure 5. Multipath propagation paths: (**a**) single reflector; (**b**) two reflectors.

R_d is a direct path between the radar and the real target, and R_m is a reflection path that passes through the target, the radar, and reflectors. The radar is expressed as O, and the plant is expressed as P. Four possible propagation paths are shown in Table 1.

Table 1. Propagation paths.

Type of Paths	Propagation Paths	Targets
R_d+ R_d	$O \to T_1 \to O$	T_1(real)
R_m+ R_d	$O \to Q \to T_1 \to O$	M_a(ghost)
R_d+ R_m	$O \to T_1 \to Q \to O$	M_b(ghost)
R_m+ R_m	$O \to Q \to T_1 \to Q \to O$	M_c(ghost)

When there is a single reflector, the propagation point $Q = P$. From Figure 5a and Table 1, it can be seen that except for the first type of the two-way direct path, the other

three are all multipath. According to the principle of specular reflection, the reflective propagation path is

$$R_{\mathrm{m}} = R_{\mathrm{m}_1} = OP + PT_1 \tag{29}$$

Due to the effect of multipath, one real target T_1 and three false targets $M_{\mathrm{a}} = M_1$, $M_{\mathrm{b}} = M_2$, $M_{\mathrm{c}} = M_3$ are detected on the radar.

When two of the plants, walls, ceilings, and floors are reflectors, the propagation points $Q = [P, Q_1]$. From Figure 5b and Table 1, it can be seen that except for the first type of the two-way direct path, the other three are all multipath. The reflective propagation path is

$$R_{\mathrm{m}_2} = OP + PQ_1 + Q_1T_1 \tag{30}$$

Due to the effect of multipath, one real target T_1 and three false targets $M_{\mathrm{a}} = M_4$, $M_{\mathrm{b}} = M_5$, $M_{\mathrm{c}} = M_6$ are detected on the radar.

6.1.2. A Human beside a Plotted Plant

Considering the case that the plant is the reflector or one of the reflectors. When the target is behind the plant and is very close to each other, the location difference between a multipath ghost target and a real target is very small. At the same time, the signal is absorbed, reflected, refracted, and scattered by plant leaves and branches in the propagation process, so the echo signal energy is greatly attenuated. Therefore, when the target is located behind the plant, it is not considered when a plant acts as a reflector.

The radar signal propagation paths under a single and two reflector(s) are the same as the case when a target is beside a plant. In each case, the radar detects one real target and three false targets due to multipath theoretically.

6.2. Multipath Suppression

Take the condition that the human is beside the plant as an example, and plants and walls act as reflectors. Indoor object positions and propagation paths are shown in Figure 6. The coordinate of the radar O is (0, 0), the line PQ_3 is perpendicular to the line T_1T_1', and the line Q_2Q_4 is perpendicular to the y-axis. Let the coordinate of the real target be (x, y) and the coordinate of the green plant be $(x_{\mathrm{plant}}, y_{\mathrm{plant}})$.

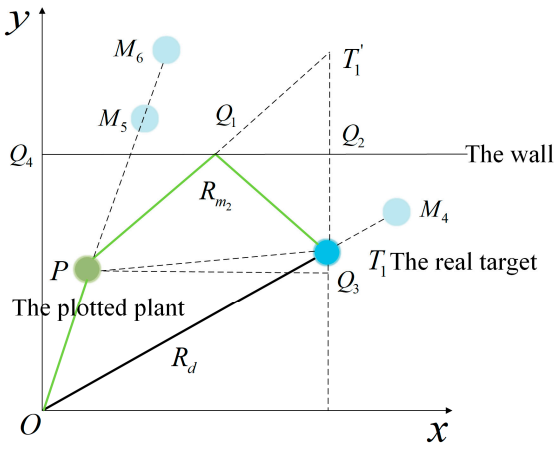

Figure 6. A radar signal propagation schematic.

As for the ghost target M_4, propagation paths are the second type $R_{\mathrm{m}} + R_{\mathrm{d}}$ in Table 1. The reflection path $R_{\mathrm{m}} = R_{\mathrm{m}_2}$, and it is equal to $OP + PQ_1 + Q_1T_1$. According to the symmetry of specular reflection, the real target T_1 has a symmetry point T_1' with respect to the wall, and $Q_1T_1 = Q_1T_1'$, $T_1T_1' = 2Q_2T_1$. Calculate the reflection path

$$\begin{aligned} R_{m_2} &= OP + PT_1' \\ &= OP + \sqrt{(PQ_3)^2 + (Q_3T_1')^2} \\ &= OP + \sqrt{(PQ_3)^2 + (Q_1T_1 + Q_2Q_3)^2} \\ &= \sqrt{x_{\text{plant}}^2 + y_{\text{plant}}^2} + \sqrt{(x - x_{\text{plant}})^2 + (2OQ_4 - y - y_{\text{plant}})^2} \end{aligned} \tag{31}$$

where the distance $OP = \sqrt{x_{\text{plant}}^2 + y_{\text{plant}}^2}$ between the radar and the plant and the distance OQ_4 between the wall and the radar in the y-axis direction are constant. They can be obtained by experiment measurements.

Thus, the distance between the radar and the false target M_4 is

$$OM_4 = 0.5(R_{m_2} + R_{\text{tar}}) \tag{32}$$

where R_{tar} denotes the distance between the real target and the radar.

As for the ghost target M_5, propagation paths are the third type $R_d + R_m$ in Table 1, the distance between the radar and the false target M_5 is $OM_5 = OM_4$.

As for the ghost target M_6, propagation paths are the fourth type $R_m + R_m$ in Table 1, the distance between the radar and the false target M_6 is

$$OM_6 = R_{m_2} \tag{33}$$

Therefore, the complete multipath removal process is

1. Difference Calculation between estimation and theory

A point in the cluster coordinate vector $\boldsymbol{x}_{\text{PosTar}}$ and $\boldsymbol{y}_{\text{PosTar}}$ is selected as a real target, and the corresponding false target information can be calculated according to the analysis above. Traverse in other cluster coordinates, and the difference between each cluster coordinate and the theoretical false target is calculated.

2. Difference Comparison

When the calculated difference is less than or equal to a set error, the selected cluster point is a true target and the matching false targets can be found.

3. Ghost Target Removal

Remove the real target and corresponding false target coordinates from cluster coordinates, and repeat the above process until all points in the cluster coordinates are removed to obtain the real target position $(\boldsymbol{x}, \boldsymbol{y})$.

7. Experiment and Result Analysis

7.1. Experiments

A 77 GHz FMCW millimeter-radar AWR1843 and DCA1000EVM were employed for the experiment provided by Texas Instruments (TI), Dallas, TX, USA. The system has an effective bandwidth of 767.539 MHz and is equipped with a 3×4 MIMO antenna array for transmitting and receiving. The pulse repetition interval is 160 µs, and the period of a frame is set to 0.062 s. In the configuration, a total of 256 samples are chosen in a chirp, the range resolution is 0.195 m, and the azimuth angle resolution at the center of the field of view is 14.324°. When the bandwidth of the radar is increased, the range resolution will be improved, and the target can be detected with higher accuracy; however, it may also make the process of system design and implementation more difficult. Because that requires better-performing transmitters, receivers, and processors. Azimuth resolution will improve when more receiving or transmitting antennas are designed for horizontal target detection.

Multiple steps were integrated, and five daily environments were analyzed totally to verify the effectiveness of the proposed scheme. Figure 7 shows the first measurement environment, and the measurement was set up in a hallway with a potted plant, such as entrances or corridors of many large buildings. Set the position of the radar as (0, 0) and the

green plant was placed at the (0.300 m, 1.200 m). There were two measurement conditions: people stood still at the back and the side of the plant. As for both measurements, people stood at a distance R from the plant center with R = 0.650 m. The authors agreed to participate in the experiments as human subjects.

(**a**) (**b**)

Figure 7. Two measurement conditions: (**a**) behind a plant; (**b**) beside a plant.

As for the CFAR detection, the number of training cells is selected as 16 in the range dimension and 4 in the Doppler dimension, and the number of guard cells is selected as 5 in the range dimension and 2 in the Doppler dimension. As for the false alarm rates, 10^{-5} and 10^{-7} are chosen in the range and Doppler dimension, respectively.

7.2. Results

To evaluate the accuracy of the proposed method, complete noise, clutter, multipath removal, and target detection are carried out. After that, the method is tested in four other different environments to check its reliability. Considering the existing human sensing algorithms, the proposed method is also compared with human detection ideas in [27,28] through two evaluation metrics.

7.2.1. Human Target Localization

The HRRPs of raw data are shown in Figure 8. After applying static filtering, Figure 9a shows that an obvious multipath peak around 3.2 m exists when the target is behind the plant. The magnitude of the peak signal is less than that of some static noise so it is only seen after static filtering. There is some time-variant clutter in the first 0.5 s when the human is beside the plant in Figure 9b. These existing phenomena will affect the target detection. Thus, further removal is necessary to improve the target detection performance.

FFT is carried out in the range and Doppler dimension, respectively, and range-Doppler maps are shown in Figure 10 when the target is behind and beside the green plant. When the human is behind the plant in Figure 10a, there are two obvious peaks that correspond to the real target and a ghost target, respectively. When the human is beside the plant in Figure 10b, there are three peaks and some clutter. Those non-target signals can be removed through the following DBSCAN algorithm.

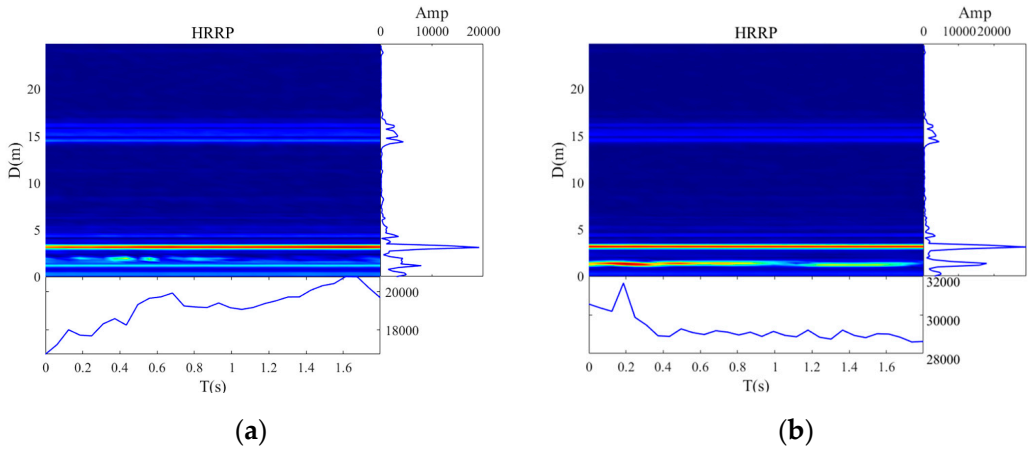

Figure 8. HRRP comparison: (**a**) HRRP before noise filtering (back); (**b**) HRRP before noise filtering (side).

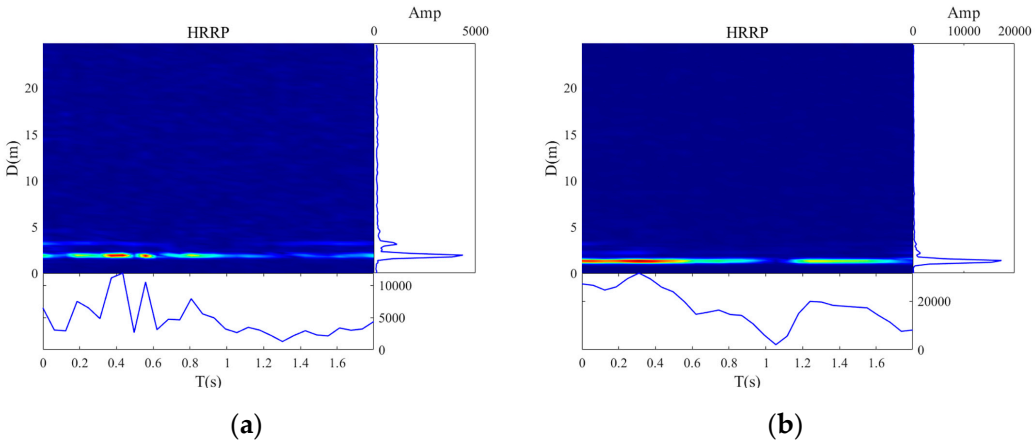

Figure 9. HRRP Comparison: (**a**) HRRP after noise filtering (back); (**b**) HRRP after noise filtering (side).

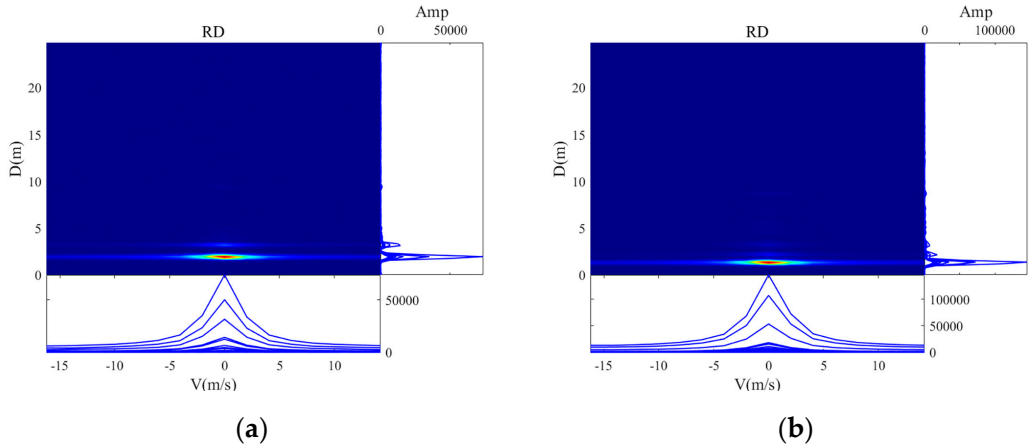

Figure 10. HRRP comparison: (**a**) RD after 2D-FFT (back); (**b**) RD after 2D-FFT (side).

When implementing the DBSCAN clustering, the parameter domain radius threshold ε is selected as 1.5 distance cells = 1.5×0.195 m ≈ 0.293 m. The minimum number (MinPts) is selected as $F/2$ which is about 15 according to the binary integration. Frames are the same for different samples. Figure 11 shows classification results obtained by DBSCAN clustering and binary integration when the human is behind and beside the plant, respectively. It

can be seen that through the DBSCAN algorithm and binary integration, points with large fluctuations or points with too few occurrences at the same position are determined as clutter. It can be removed then to effectively mitigate time-variant non-target signals.

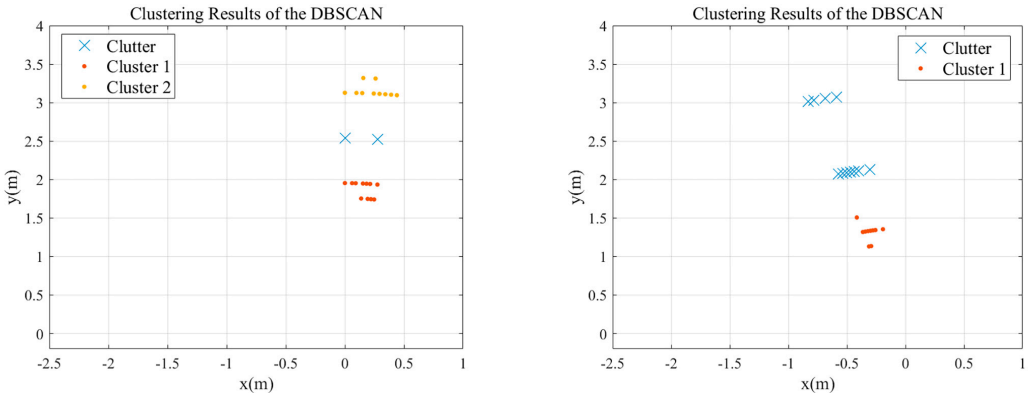

(**a**) (**b**)

Figure 11. Detection point distribution of near a plant: (**a**) After Classification (back); (**b**) After Classification (side).

When a human is beside the plant, the multipath effect is not obvious. Through the DBSCAN algorithm and binary integration, the human can be detected directly. When a human is behind the plant, it can be seen that a multipath point exists. The characteristics of the multipath ghost targets and real targets are similar, and the DBSCAN algorithm determines them both as clusters, which need to be removed further.

The position of the real target is obtained by multipath suppression. In Figure 12, blue squares show the position information of all possible targets before multipath suppression, and orange triangles show the real target position obtained by multipath suppression. Comparing the theoretical positions of false targets with possible targets in Figure 12, it can be seen that the false target is removed while the real target point is retained.

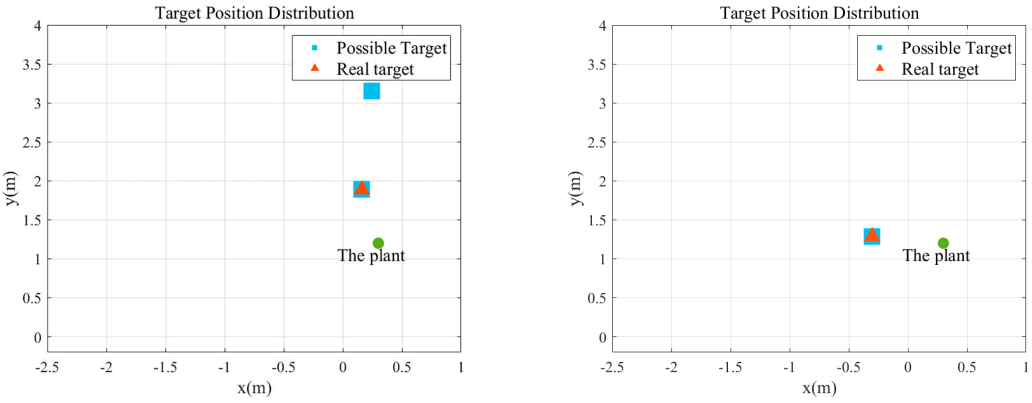

(**a**) (**b**)

Figure 12. Target Point Distribution: (**a**) Targets behind the Plant; (**b**) Targets beside the Plant.

When the human is behind the plant, the human is detected at (0.161 m, 1.888 m). When the human is beside the plant, the detected human is at the (−0.302 m, 1.289 m). Comparing the estimated position of the target human after multipath suppression with the actual data, average errors all within 0.195 m. That is reasonable due to human sway and body width. The estimated position of the target is close to the real value, which indicates that the adopted method is effective, and the detected target is the real human target.

7.2.2. Target Detection in Different Environments

To evaluate the reliability of the clutter removal and multipath mitigation method, experiments are carried out further in four other indoor complex environments.

As for the green plants, a different variety of green plants was selected, ensuring a thorough analysis of how different quantities and types of green plants might affect the measurements. This aimed to mimic real-life scenarios where various types of green plants are commonly found in indoor environments. The measurement was set with one and two potted plants, respectively, in a hallway, as shown in Figure 13.

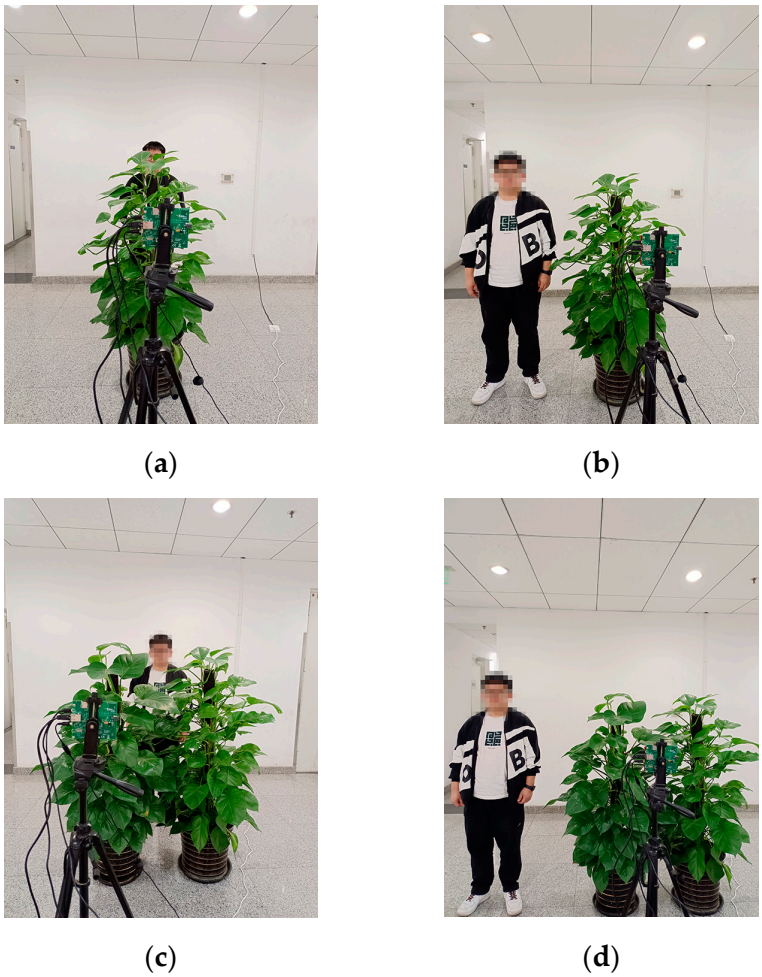

Figure 13. Four measurement scenarios: (**a**) behind a new plant; (**b**) beside a new plant; (**c**) behind two new plants; (**d**) beside two new plants.

After applying the static filtering and range-FFT, four HRRPs are gained. Figure 14a–d show that there exist multipath signals and a little time-varying clutter.

As shown in Figure 15, the detection points are divided into clusters and clutter through the DBSCAN algorithm. It can be seen that point distribution and detection results are similar for the newly chosen plant in Figure 13a,b and the first kind of plant in Figure 7. However, there are more clutter points, and target points have larger fluctuations when increasing the number of green plants. This can be solved after the DBSCAN clustering and binary integration.

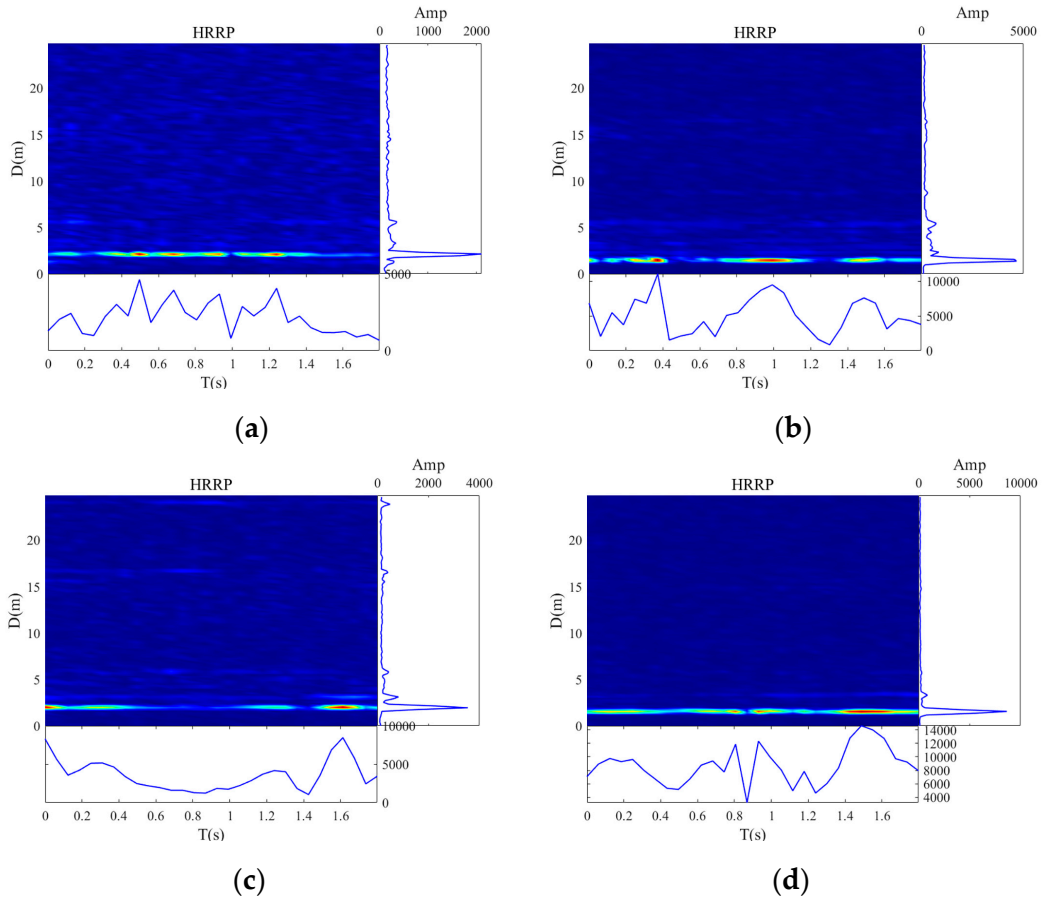

Figure 14. HRRP comparison: (**a**) HRRP after noise filtering for one plant (back); (**b**) HRRP after noise filtering for one plant (side); (**c**) HRRP after noise filtering for two plants (back); (**d**) HRRP after noise filtering for two plants (side).

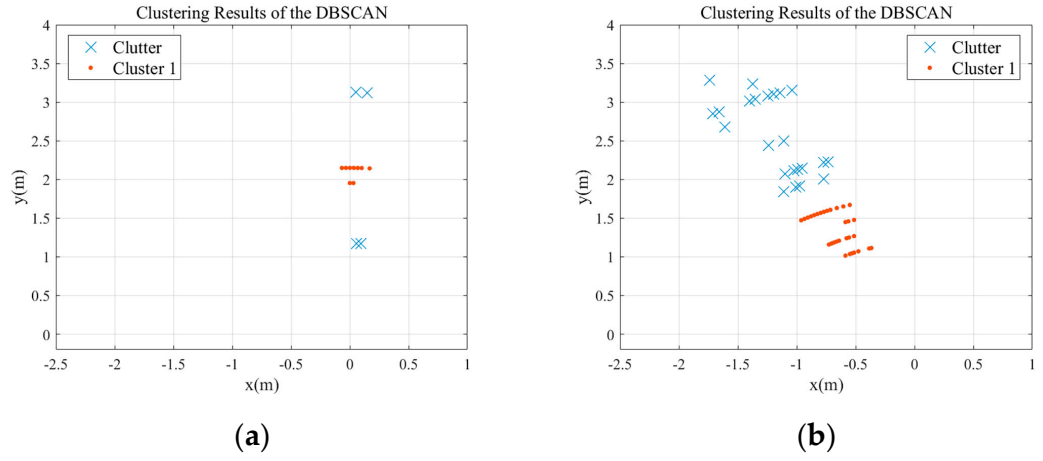

Figure 15. *Cont*.

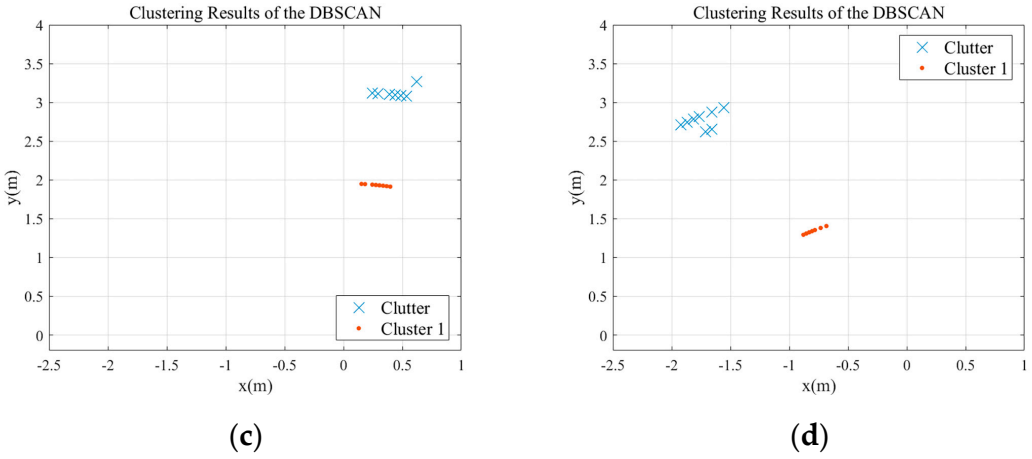

Figure 15. Detection point distribution: (**a**) after classification for one plant (back); (**b**) after classification for one plant (side); (**c**) after classification for two plants (back); (**d**) after classification for two plants (side).

Figure 16 shows possible target distribution and real target distribution. The detection average errors are within a reasonable range of 0.195 m.

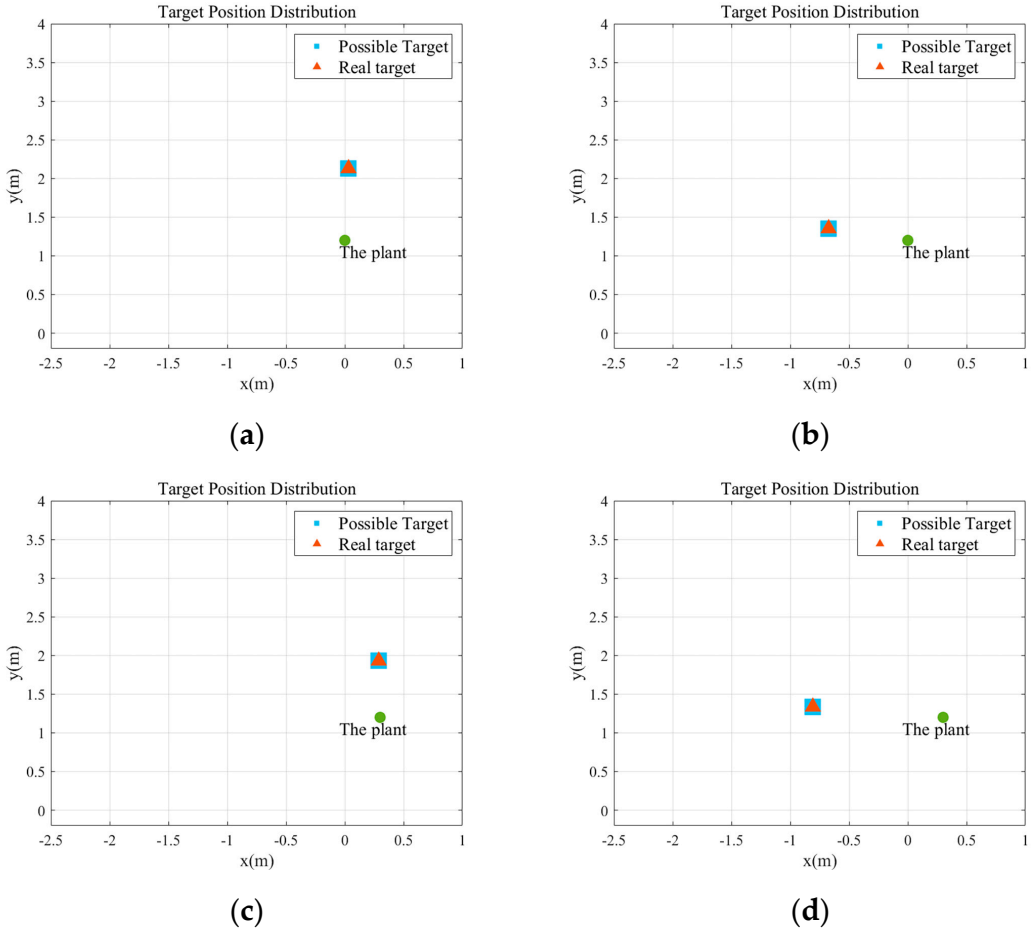

Figure 16. Target point distribution: (**a**) targets behind one plant; (**b**) targets beside one plant; (**c**) targets behind two plants; (**d**) targets beside two plants.

As for other complex environments, two measurement scenes such as a break room and a meeting room were selected. Figure 17a shows a standing human in a break room with curtains and Figure 17b shows a sitting human in a meeting room with a desk and chairs.

(**a**) (**b**)

Figure 17. Two measurement scenarios: (**a**) beside curtains; (**b**) behind furniture.

Set the position of the radar as (0, 0). As for the first measurement condition, people stayed at a linear distance R from the radar center with R = 2.300 m. The linear distance R from the radar center equals 2.750 m for the second condition.

After applying the static filtering and range-FFT, two HRRPs are gained. Figure 18a,b show that more time-varying clutter exists than in the experiments with green plants before. Target signals spread to adjacent range cells.

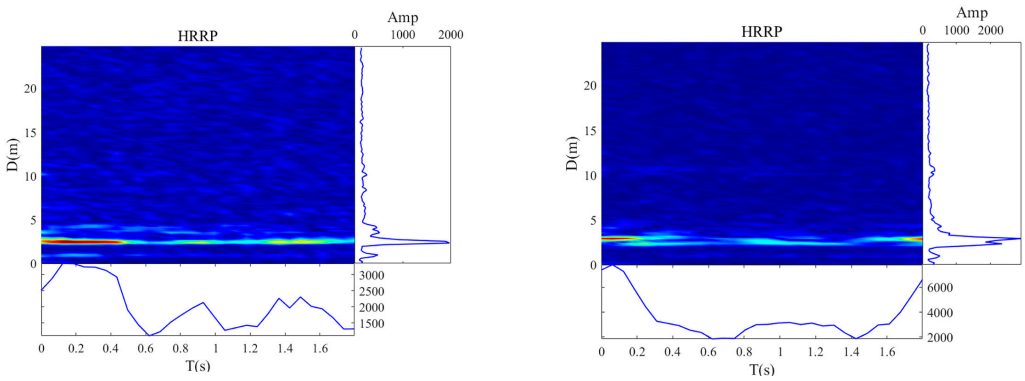

(**a**) (**b**)

Figure 18. HRRP comparison after noise filtering: (**a**) HRRP (beside curtains); (**b**) HRRP (behind furniture).

As shown in Figure 19, the detected points are classified into clusters and clutter. It can be seen that points have larger fluctuations. The DBSCAN algorithm can distinguish the real targets from all possible points.

Figure 20 shows possible target distribution and real target distribution. The detection average errors are within the reasonable range.

Compare average errors in different environments as shown in Figure 21. It can be seen that the average errors of detection results in 5 environments are all within 0.195 m. The analysis shows that there is no significant difference in the errors across different environments, and the overall average error is consistently low. This demonstrates that the static human detection method performs reliably and accurately.

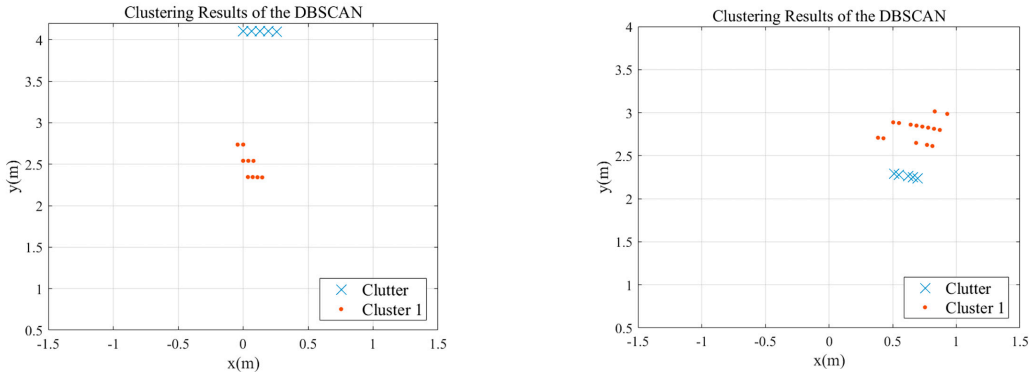

(**a**) (**b**)

Figure 19. Detection point distribution of complex environments: (**a**) after classification (back); (**b**) after classification (side).

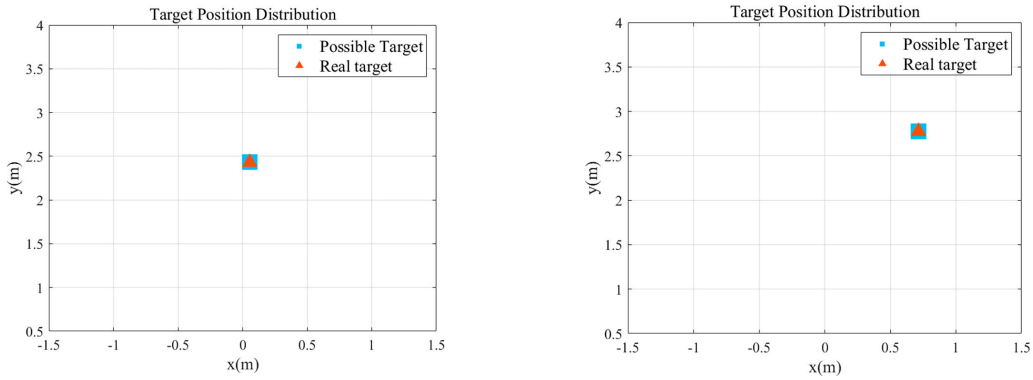

(**a**) (**b**)

Figure 20. Target point distribution: (**a**) targets beside curtains; (**b**) targets behind furniture.

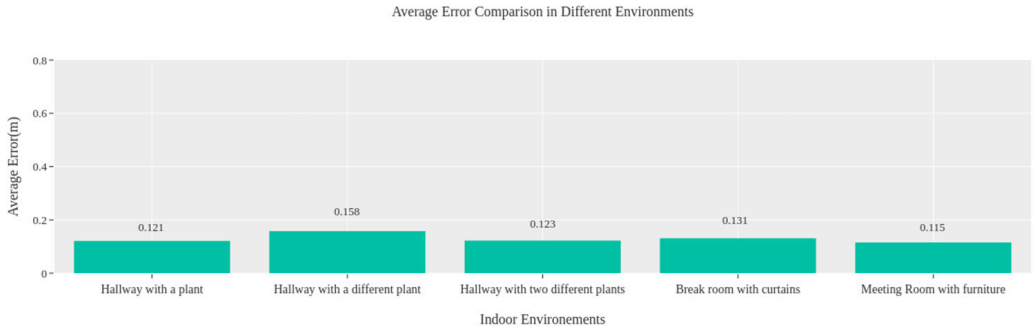

Figure 21. Average error comparison in different environments.

7.2.3. Method Comparison

Compare the proposed method with human detection using the EABS and a window filter in [27], Doppler-compensated human detection in [28], and human localization and multipath cancellation in [21]. Set the false alarm probability as 0.01. Compare four methods in non-target signal removal, including static noise, time-varying clutter, and multipath ghost targets. The result is shown in Table 2. It can be seen that the proposed method is the most comprehensive among these four detection methods. It considers multiple static, clutter, and multipath signals mitigation according to characteristics of static human targets, thus resulting in a more robust localization.

Table 2. Method performance comparison in non-target signal removal.

Methods	Static Noise	Time-Varying Clutter	Multipath
The human detection method in [27]	Removed	Partly removed	Not removed
The static human detection in [28]	Removed	Partly removed	Not removed
Human localization in urban roads [21]	Removed	Not removed	Removed
The proposed method	Removed	Removed	Removed

Then, two evaluation metrics are used to evaluate detection accuracy and reliability, i.e., correct detection rate (CDR) and miss detection rate (MDR). The evaluation results are shown in Table 3 (human behind the plant) and Table 4 (human beside the plant) for the scene in Figure 7.

Table 3. Comparison results (human behind the plant).

Methods	CDR	MDR
The human detection method in [27]	14.931%	85.069%
The static human detection in [28]	62.847%	37.153%
Human localization in urban roads [21]	75.412%	24.588%
The proposed method	81.250%	18.750%

Table 4. Comparison results (human beside the plant).

Methods	CDR	MDR
The human detection method in [27]	77.714%	22.286%
The static human detection in [28]	67.714%	38.286%
Human localization in urban roads [21]	84.620%	15.380%
The proposed method	90.286%	9.714%

It can be seen that both the detection probability and miss alarm probability have a better performance for the proposed human detection and localization method. Firstly, the method considers the effect of time-variant clutter generated by the complex structure of a plant and the occasionally unstable radar. This can improve human detection and localization accuracy. So, the proposed method performs with a higher CDR than the method in [21]. Secondly, the method in [27] assigns 1 for an existing target and 0 for no target for the OS-CFAR detection. Then, a target may occupy multiple range cells with corresponding signals having the same signal magnitudes. A window filter can tackle the influence; however, sometimes, the situation still exists because the difference between signal magnitudes is still not very obvious. The proposed method remains unchanged for an existing target and 0 for no target in the CFAR detection, so the miss alarm probability can be lower. Finally, the method in [28] calculates a Doppler-compensated angle to mitigate signal fluctuation due to breathing. Through it, algorithm accuracy can be improved. The proposed method also tackles the problem through the Capon algorithm, and it removes some time-variant clutter at the same time.

8. Conclusions

A method was explored to detect and locate a static human indoors using a millimeter-wave radar. Static noise was removed through static filtering, and the CFAR algorithm was used to detect the human. To suppress time-variant clutter, a method combined with the DBSCAN algorithm with binary integration was proposed. Time accumulation with the DBSCAN algorithm was innovatively used as the signal strength of static human

targets is relatively low. Binary integration could improve the detection robustness. As for ghost targets, four cases were considered: one reflector, two reflectors, a target behind an obstacle, and a target beside an obstacle. Finally, the location of the human target was estimated by combining the distance and azimuth angle information. The experiment was carried out in five different indoor complex environments considering green plants, curtains, and furniture, and results show that the proposed method is effective within an average error of 0.195 m to mitigate noise, time-variant clutter, and multipath, and localize a static human. Meanwhile, the experiment results show that the method can have a better detection probability than the conventional methods.

In the future, estimation of room sizes can be explored as the current human detection depends on some prior knowledge of rooms. This will improve the adaptability of the current method. As for the computational complexity of the proposed method, the averaging filtering is simple to calculate and has a complexity of $O(N)$. As for time-varying clutter removal, the DBSCAN algorithm has a complexity of $O(N^2)$. The multipath matching technique has a calculation complexity of $O(N)$. The DBSCAN algorithm has a higher computational complexity and can be improved through using multithreading or multiprocessing techniques. Computational tasks can be distributed across multiple processor cores, and the overall computation can be faster.

Author Contributions: Conceptualization, P.C.; Methodology, Z.X.; Software, Y.B. and J.S.; Validation, L.T.; Investigation, Z.X.; Resources, P.C., J.W., Y.B., J.S. and L.T.; Writing—original draft, Z.X.; Writing—review & editing, P.C.; Supervision, J.W.; Project administration, P.C. All authors have read and agreed to the published version of the manuscript.

Funding: This research was funded in part by the Open Fund of Qianjiang Laboratory, Hangzhou Innovation Institute, Beihang University, under Grant 2020-Y7-A-010.

Data Availability Statement: The original contributions presented in the study are included in the article, further inquiries can be directed to the corresponding author.

Conflicts of Interest: The authors declare no conflicts of interest.

References

1. Han, R.; Feng, W.; Wang, F.; Qian, Z.; Yan, H.; Wang, S. Benchmarking the Complementary-View Multi-Human Association and Tracking. *Int. J. Comput. Vis.* **2024**, *132*, 118–136. [CrossRef]
2. Jiang, Y.; Gong, T.; He, L.; Yan, S.; Wu, X.; Liu, J. Fall Detection on Embedded Platform Using Infrared Array Sensor for Healthcare Applications. *Neural Comput. Appl.* **2024**, *36*, 5093–5108. [CrossRef]
3. Wu, L.; Huang, C.; Fei, L.; Zhao, S.; Zhao, J.; Cui, Z.; Xu, Y. Video-Based Fall Detection Using Human Pose and Constrained Generative Adversarial Network. *IEEE Trans. Circuits Syst. Video Technol.* **2024**, *34*, 2179–2194. [CrossRef]
4. Wang, S.; Liu, B.; Wang, Y.-L.; Hu, Y.; Liu, J.; He, X.-D.; Yuan, J.; Wu, Q. Machine-Learning-Based Human Motion Recognition via Wearable Plastic-Fiber Sensing System. *IEEE Internet Things J.* **2023**, *10*, 17893–17904. [CrossRef]
5. Lattanzi, E.; Calisti, L.; Capellacci, P. Lightweight Accurate Trigger to Reduce Power Consumption in Sensor-Based Continuous Human Activity Recognition. *Pervasive Mob. Comput.* **2023**, *96*, 101848. [CrossRef]
6. Pyun, K.R.; Kwon, K.; Yoo, M.J.; Kim, K.K.; Gong, D.; Yeo, W.-H.; Han, S.; Ko, S.H. Machine-Learned Wearable Sensors for Real-Time Hand-Motion Recognition: Toward Practical Applications. *Natl. Sci. Rev.* **2024**, *11*, nwad298. [CrossRef] [PubMed]
7. He, Y.; Li, X.; Jing, X. A Mutiscale Residual Attention Network for Multitask Learning of Human Activity Using Radar Micro-Doppler Signatures. *Remote Sens.* **2019**, *11*, 2584. [CrossRef]
8. Luo, H.; Zhang, W.; Ren, Z.; Tang, C.; Ou, Y.; Cui, G.; Guo, S. Analysis of Electromagnetic Wave and Multipath Suppression from Overhead Perspective. *Remote Sens.* **2023**, *15*, 4903. [CrossRef]
9. Gianoglio, C.; Mohanna, A.; Rizik, A.; Moroney, L.; Valle, M. On Edge Human Action Recognition Using Radar-Based Sensing and Deep Learning. *IEEE Trans. Ind. Inform.* **2024**, *20*, 4160–4172. [CrossRef]
10. Liang, Z.; Jin, Y.; Yang, D.; Liang, B.; Mo, J. Two-Step Accuracy Improvement for Multitarget Detection in Complex Environment Using UWB Radar. *Remote Sens.* **2024**, *16*, 877. [CrossRef]
11. Raeis, H.; Kazemi, M.; Shirmohammadi, S. CAE-MAS: Convolutional Autoencoder Interference Cancellation for Multiperson Activity Sensing With FMCW Microwave Radar. *IEEE Trans. Instrum. Meas.* **2024**, *73*, 8001710. [CrossRef]
12. Zhou, X.; Jin, T.; Dai, Y.; Song, Y.; Li, K. Three-Dimensional Human Pose Estimation from Micro-Doppler Signature Based on SISO UWB Radar. *Remote Sens.* **2024**, *16*, 1295. [CrossRef]
13. Chen, B.; Chen, Y.; Fu, Y.; Yang, F. Multipath Model and Ghost Suppression for Millimeter Wave Road Monitoring Radar. *J. Anhui Univ. Technol.* **2023**, *40*, 324–332. [CrossRef]

14. Jeong, T.; Lee, S. Ghost Target Suppression Using Deep Neural Network in Radar-Based Indoor Environment Mapping. *IEEE Sens. J.* **2022**, *22*, 14378–14386. [CrossRef]
15. Shi, J.; Hu, G.; Zhou, H. Entropy-Based Multipath Detection Model for MIMO Radar. *J. Syst. Eng. Electron.* **2017**, *28*, 51–57. [CrossRef]
16. Sasakawa, D.; Honma, N.; Nakayama, T.; Iizuka, S. Fast Living-Body Localization Algorithm for MIMO Radar in Multipath Environment. *IEEE Trans. Antennas Propag.* **2018**, *66*, 7273–7281. [CrossRef]
17. Yu, K.; Wen, K.; Li, Y.; Zhang, S.; Zhang, K. A Novel NLOS Mitigation Algorithm for UWB Localization in Harsh Indoor Environments. *IEEE Trans. Veh. Technol.* **2019**, *68*, 686–699. [CrossRef]
18. Feng, R.; Greef, E.D.; Rykunov, M.; Sahli, H.; Pollin, S.; Bourdoux, A. Multipath Ghost Recognition for Indoor MIMO Radar. *IEEE Trans. Geosci. Remote Sens.* **2022**, *60*, 5104610. [CrossRef]
19. Li, Y.; Li, Y.; Wang, Y.; Lin, Y.; Shen, W.; Jiang, W.; Sun, J. HCM-LMB Filter: Pedestrian Number Estimation with Millimeter-Wave Radar in Closed Spaces. *Remote Sens.* **2023**, *15*, 4698. [CrossRef]
20. Hao, Z.; Yan, H.; Dang, X.; Ma, Z.; Jin, P.; Ke, W. Millimeter-Wave Radar Localization Using Indoor Multipath Effect. *Sensors* **2022**, *22*, 5671. [CrossRef]
21. Zheng, J.Y.; Wu, P.L.; Chen, J.H.; Guo, S.S.; Cui, G.L. Vehicle-Mounted Millimetre-Wave Radar Multipath False-Target Analysis and Cancellation Method. *Syst. Eng. Electron.* **2024**, *46*, 88–96.
22. Lei, P.Z.; Fan, C.Y.; Huang, X.T.; Zhu, J.H. Weak Moving Target Detection with Multipath Clutter Suppression Based on Hough Transform. In Proceedings of the 2013 14th International Radar Symposium (IRS), Dresden, Germany, 19–21 June 2013; Volume 2, pp. 774–778.
23. Liang, J.; Liang, Q.L. Outdoor Propagation Channel Modeling in Foliage Environment. *IEEE Trans. Veh. Technol.* **2010**, *59*, 2243–2252. [CrossRef]
24. In, C.; Lim, D.-W.; Kang, J.-M.; Lee, J.-H.; Kim, H.-M.; Kim, S.; Kim, C. Human Detection Based on the Condition Number in the Non-Stationary Clutter Environment Using UWB Impulse Radar. In Proceedings of the 2013 Asia-Pacific Microwave Conference Proceedings (APMC), Seoul, Republic of Korea, 5–8 November 2013; IEEE: Seoul, Republic of Korea, 2013; pp. 1006–1008.
25. Zhong, Y.; Yang, Y.; Zhu, X.; Dutkiewicz, E.; Zhou, Z.; Jiang, T. Device-Free Sensing for Personnel Detection in a Foliage Environment. *IEEE Geosci. Remote Sens. Lett.* **2017**, *14*, 921–925. [CrossRef]
26. Lei, P.; Huang, X.; Fan, C.; Ji, K.; Qin, X. Moving Human Target Detection in Foliage Environments Based on Hough Transform. In Proceedings of the 2013 IEEE International Geoscience and Remote Sensing Symposium—IGARSS, Melbourne, Australia, 21–26 July 2013; IEEE: Melbourne, Australia, 2013; pp. 2637–2640.
27. Zhang, J.; Jin, T.; He, Y.; Qiu, L.; Zhou, Z.M. Foliage-Penetration Human Tracking by Multistatic Radar. In Proceedings of the 2016 IEEE International Geoscience and Remote Sensing Symposium (IGARSS), Beijing, China, 10–15 July 2016; IEEE: Beijing, China, 2016; pp. 6102–6105.
28. Will, C.; Vaishnav, P.; Chakraborty, A.; Santra, A. Human Target Detection, Tracking, and Classification Using 24-GHz FMCW Radar. *IEEE Sens. J.* **2019**, *19*, 7283–7299. [CrossRef]
29. Guleryuz, O.G. Weighted Averaging for Denoising With Overcomplete Dictionaries. *IEEE Trans. Image Process.* **2007**, *16*, 3020–3034. [CrossRef] [PubMed]
30. Danielson, G.C.; Lanczos, C. Some Improvements in Practical Fourier Analysis and Their Application to X-Ray Scattering from Liquids. *J. Frankl. Inst.* **1942**, *233*, 365–380. [CrossRef]
31. Nitzberg, R. Constant-False-Alarm-Rate Signal Processors for Several Types of Interference. *IEEE Trans. Aerosp. Electron. Syst.* **1972**, *AES-8*, 27–34. [CrossRef]
32. Ventzas, D.; Petrellis, N. Peak Searching Algorithms and Applications. In Proceedings of the IASTED International Conference on Signal and Image Processing and Applications, Crete, Greece, 22–24 June 2011.
33. Sun, H.; Brigui, F.; Lesturgie, M. Analysis and Comparison of MIMO Radar Waveforms. In Proceedings of the International Radar Conference, Lille, France, 13–17 October 2014; pp. 1–6.
34. Zhang, W.; Liu, T.; Yang, G.; Jiang, C.; Hu, Y.; Lan, T.; Zhao, Z. A Novel Method for Improving Quality of Oblique Incidence Sounding Ionograms Based on Eigenspace-Based Beamforming Technology and Capon High-Resolution Range Profile. *Remote Sens.* **2022**, *14*, 4305. [CrossRef]
35. Ester, M.; Sander, J.; Kriegel, H.P.; Xu, X. A Density-Based Algorithm for Discovering Clusters in Large Spatial Databases with Noise. In Proceedings of the 2nd International Conference on Knowledge Discovery and Data Mining, Portland, OR, USA, 2–4 August 1996.
36. Mark, A. Richards Binary Integration. In *Fundamentals of Radar Signal Processing*; McGraw Hill: New York, NY, USA, 2014; pp. 491–495.
37. Jebari, S.; Smiti, A.; Louati, A. AF-DBSCAN: An Unsupervised Automatic Fuzzy Clustering Method Based on DBSCAN Approach. In Proceedings of the 2019 IEEE International Work Conference on Bioinspired Intelligence (IWOBI), Budapest, Hungary, 3–5 July 2019; pp. 1–6.